Carnot Battery Analysis for Mobile Camps

Sushrut Deshpande[a,b], Antoine Laterre[c], Maarten Vergote[a], Bart Janssens[a] and Vincent Lemort[c]

[a] *Royal Military Academy, Brussels, Belgium, sushrut.deshpande@mil.be*
[b] *University of Liege, Liege, Belgium,*
[c] *Université catholique de Louvain, Louvain-la-Neuve, Belgium,*

Abstract:
Mobile camps—such as military forward operating bases and humanitarian relief camps—operate at relatively small scales and are often deployed in hazardous or resource-constrained environments. This increases the need of self-reliance of the camp which needs to be met by easily deployable renewables like PV panels. In such contexts, the choice of energy storage technology is critical, as it must balance performance, robustness, and mobility. Carnot Batteries, which combine heat pump, thermal storage, and power cycle, have recently emerged as an possible alternative to conventional energy storage systems such as electro-chemical battery, particularly due to their ability to utilize locally available storage materials such as water.
This work investigates the feasibility of a low-temperature ($90 - 95^0$C) Carnot Battery tailored for mobile camp applications characterized by power capacities, where mobility and logistical constraints are major design considerations. Because the thermal storage medium (e.g., water) can typically be sourced on-site, the carried components of the system are limited to the energy-generating unit (PV panels), the charging unit Heat Pump, the thermal energy storage containment, and the Organic Rankine Cycle. The study proposes a methodology to determine an optimal thermodynamic design point along with the energy dispatch modelling which combines the thermodynamics of the Carnot Battery to the energy system of the camp.
The results show that the optimal design is strongly influenced by system-level constraints, particularly mass and thermal energy storage volume limitations. While the round-trip efficiency remains relatively stable, the energy density becomes the dominant factor in determining the optimal design as constraints become active. Furthermore, the integration of Carnot Battery becomes most relevant when conventional lithium-ion storage reaches its capacity limits due to hazardous aspects of chemical energy storages. The results also highlight the strong coupling between component sizing and dispatch dynamics, with the Organic Rankine Cycle playing a critical role in minimizing fuel consumption. Overall, the study demonstrates that Carnot batteries can be relevant under strict mobility constraints; however, this advantage holds only when additional energy generation systems, such as photovoltaic panels, are excluded from the containerised system.

Keywords:
Thermodynamics; Energy; Carnot Battery, Mobile Energy Camp.

1. Introduction

In recent years, Heat pump (HP) – Organic Rankine Cycle (ORC) based Carnot batteries (CB) have attracted significant interest as a cost-effective and environmentally friendly energy storage technology [1, 2, 6]. This work explores the potential of this technology as an energy storage solution for the electrification of mobile base camps.
The primary objective of this paper is to propose a design-point sizing methodology that integrates the optimal thermodynamic design of the Carnot battery with the optimal sizing and dispatch of a mobile camp's energy system. Chemical batteries are known to pose safety risks, particularly under mobile operating conditions; therefore, investigating a Carnot battery-based system for this application is well justified. The safety hazardous of Chemical batteries enforces the maximum carry able capacity generally less than 50 kWh.

Several general frameworks exist for sizing microgrids based on the minimisation of installation and operational costs, such as HOMER Pro [4], Microgrids.jl [5], MicroGridsPy [8], and the Microgrid Design Toolkit [3]. This work builds on similar principles, extending them to the sizing of mobile base camps using Carnot batteries, while incorporating key performance indicators relevant to such applications like electrical energy density and round trip efficiency. It combines the thermodynamic design point of CB to the optimal energy dispatch inside the microgrid.

Such a system is strongly constrained by mobility, which limits the allowable size and configuration of individual components. A schematic of the system is presented in Figures 1 and 2. All energy storage units must be integrated within the mobile platform.
As the focus of this work is on the analysis of the Carnot battery configuration, only the energy storage components are modelled in detail, while the energy generation units are parametrised. The containerised system includes the following components: a lithium-ion battery, a heat pump (HP), an organic Rankine cycle (ORC), and thermal energy storage (TES) excluding the storage medium. The latter three components together constitute the Carnot battery system.
The TES medium is assumed to be water, which can be sourced locally. This eliminates the need to transport the storage material, thereby reducing the overall system weight and improving mobility.

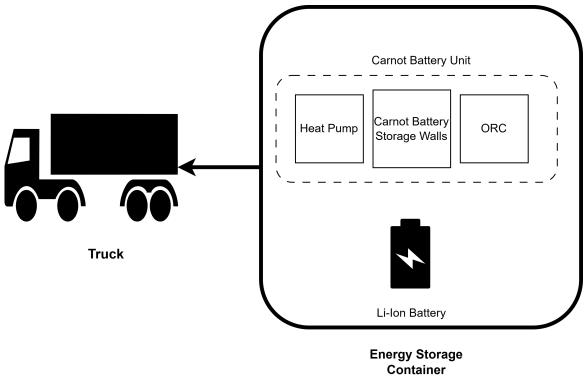

Figure 1: Energy Storage Container

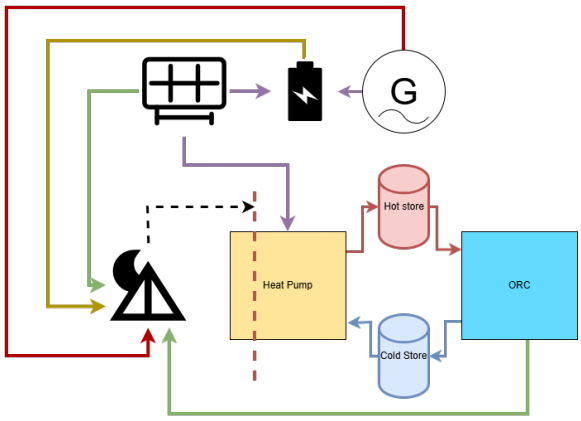

Figure 2: Camp's Energy Layout

The goal of this work is to check the impact of such a system purely for electrification application under constrained physical sizing.

2. Mathematical Modelling

This section describes the modelling techniques and methodologies chosen for the analysis. This section is split in three parts, general description of the problem 2.1., thermodynamic modelling and optimization of Carnot Battery performance 2.2., and the energy system sizing and dispatch modelling of the camp 2.3.. The modelling and simulation of the code is done is Julia [20].

2.1. Problem Description

As described in Section 1., the case study focuses on the sizing of mobile camps equipped with a CB unit. The expected electrical load profiles, specific PV production (kW/m^2), and ambient temperature of the camp are assumed to be known over the time horizon. The choice of thermal storage container is high-density polythene (HDPE) [19], while that of the TES medium is water. The storage medium is locally sourced. Given the mass allowance of the container unit, the goal is to optimally size the Carnot Battery unit and its dispatch under mass allowance.

2.2. Thermodynamic Modelling

For the thermodynamic modelling of the heat pump (HP) and organic Rankine cycle (ORC) units, the package ThermoCycleGlides.jl [9] is employed. It uses Clapeyron.jl [10] as the thermodynamic back-end for fluid property calculations. The selected equation of state is the consistent Peng–Robinson formulation [14].

This section describes the implementation of the thermodynamic components. The objective is to map the relevant Carnot battery key performance indicators (KPIs) mainly round-trip efficiency and electrical energy density, such that they can be effectively integrated into the larger-scale energy system model.

A schematic of the overall energy system layout is shown in Figure 2 and of the Carnot Battery cycle in Figure 3.

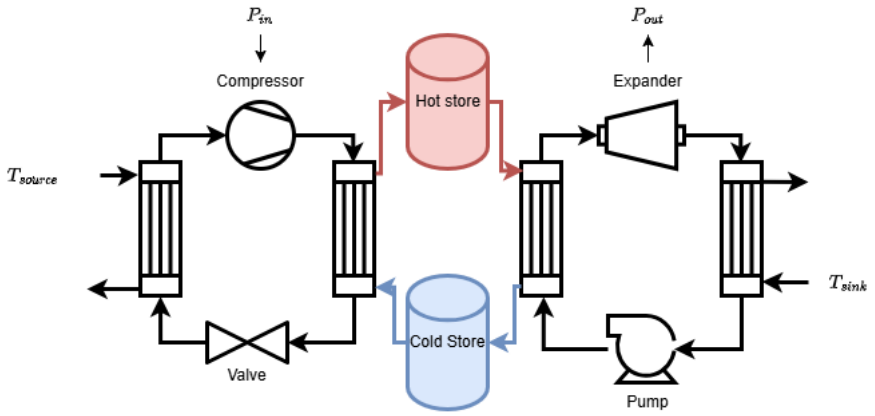

Figure 3: Carnot Battery Set Up

The expander and compressor are modelled using constant isentropic efficiencies. For the compressor:

$$\eta_c = \frac{h_{2s} - h_1}{h_{2a} - h_1}, \tag{1}$$

For the expander:

$$\eta_{exp} = \frac{h_1 - h_{2a}}{h_1 - h_{2s}}, \tag{2}$$

The heat exchangers are modelled using pinch point temperature constraints. The coefficient of performance (COP) of the HP is define as:

$$COP = \frac{\dot{Q}_{cond}}{\dot{W}_{comp}} \tag{3}$$

and the efficiency of the ORC is define as:

$$\eta_{orc} = \frac{\dot{W}_{exp} - \dot{W}_{pump}}{\dot{Q}_{evap}} \tag{4}$$

The efficiency of the Carnot Battery is computed as:

$$\eta_{CB} = COP \cdot \eta_{storage} \cdot \eta_{ORC}, \tag{5}$$

While the electrical energy density (kWh/m^3) is given by:

$$\rho_{ele} = \rho_{water} \cdot C_{p,water} \cdot (T_{hot} - T_{cold}) \cdot \eta_{ORC}, \tag{6}$$

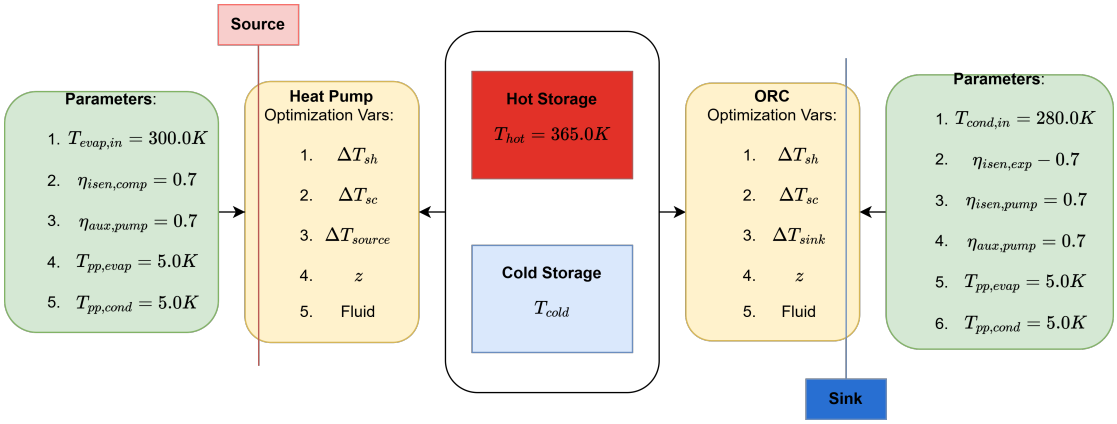

Figure 4: Carnot Battery Optimization Variables

2.2.1. Carnot Battery Performance Map

The efficiencies of both the HP and the ORC are characterised as functions of the thermal storage temperature configuration, working fluid, mole fraction (z - in the case of mixtures), and the degrees of superheating and subcooling. A schematic representation of these dependencies is shown in Figure 4. Where ΔT_{sh} and ΔT_{sc} resemble the super heating and sub cooling temperatures. ΔT_{source} resembles the glide on the evaporator of the HP while ΔT_{sink} is the glide on the condenser of the ORC. z is the molar composition of the mixture.

As the dimensionality of the variable space increases, it becomes computationally efficient to generate an optimised performance map of the Carnot battery subsystem and pass it to the system-level energy model. In this work, the optimised map is parameterised as a function of the cold storage temperature. Based on the performance maps reported by Laterre [6], acetone and isopentane are identified as optimal working fluids within the considered temperature range around 365 K. Furthermore, the use of fluid mixtures can enhance the performance of both HP systems [22] and ORC systems [23].

As phase change in mixtures is non-isothermal, the pinch point may occur within the two-phase region. To accurately capture this behaviour, the heat exchangers are discretised into 20 control volumes with equal enthalpy increments, ensuring proper resolution of pinch-point constraints [22]. This method of modelling allows the construction of optimized performance map of the thermodynamic cycle by fixing the fluid combination while optimizing for the mole fraction and super and sub cooling temperatures. Metaheuristic algorithm, Evolutionary Centers Algorithm, from Metaheuristics.jl [21] is used for optimizing the thermodynamic cycle. Both the ORC and HP cycles are optimized independently for the chosen storage configuration as shown in figure 4.

$$COP = f\left(T_{cold}, T_{hot}, \text{fluid}\ , z, \Delta T_{sh}, \Delta T_{sc}\right) \tag{7}$$

$$\eta_{ORC} = g\left(T_{cold}, T_{hot}, \text{fluid}\ , z, \Delta T_{sh}, \Delta T_{sc}\right) \tag{8}$$

In Figure 5, the Pareto front of the Carnot Battery's efficiency-density curve is shown for chosen parameters in Figure 4. The surrogate models representing the system performance, given by Equations 7 and 8, are fitted using Chebyshev polynomials.

2.3. Energy System Modelling

The energy storage is composed of a Li-Ion Battery and a CB. The generator set and PV installations are parametrised. The performances of the components apart from the CB are taken from the manufacturers. The generator load fraction to fuel consumption relations are generated over data provided by the manufacturer [18]. Along with this, the physical sizes of the components are also derived from manufacturers who provide plug-and-play type units [15] [16] [17].

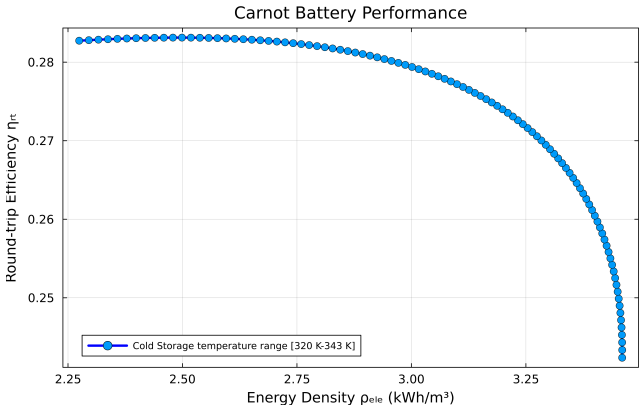

Figure 5: Carnot Battery Density Efficiency Pareto front

The energy system modelling is based on an optimal dispatch strategy for the minimisation of fuel consumption over the horizon time as described in equation 9.

$$\min_{S,P} \log\left(\frac{\int_{\mathcal{T}} \left(\text{Fuel}\left(S, P\left(t\right)\right)\right) dt}{\text{Fuel}_{\text{max}}}\right), \tag{9}$$

Where the decision variables are split into two parts. First, S is the sizing variable of the Lithium Ion battery (kWh), volume of the TES (m^3), nominal power of the HP and ORC unit (kW), and the cold storage temperature (K). Second P, are the dispatch variables per hour from all the energy sources and storages. Namely, PV, Li-Ion, generator, HP, and ORC.

$$S = \{S_{LI},\ S_{TES},\ S_{HP}^{\text{nom}},\ S_{ORC}^{\text{nom}}\ , T_{cold}\} \tag{10}$$

$$P(t) = \left\{P_{PV}(t),\ P_{LI}^{ch}(t),\ P_{LI}^{dis}(t), P_{HP}(t),\ P_{ORC}(t),\ P_G(t)\right\} \tag{11}$$

The system is constrained such that power generation at any given point is more than the demand:

$$P_{PV}(t) + P_{ORC}(t) + P_{LI}^{dis}(t) + P_G(t) \geq Load(t) + P_{LI}^{ch}(t) + P_{HP}(t), \quad \forall t \in \mathcal{T} \tag{12}$$

The output of the generator at any given time is between 0 and its maximum power rating.

$$0 \leq P_G(t) \leq S_G \tag{13}$$

As described in the previous section 2.1., the mass of the energy storage system is constrained. This is described in equation 14.

$$M(S_{LI}) + M(S_{TES}) + M(P_{HP}^{\text{nom}}) + M(P_{ORC}^{\text{nom}}) \leq M_{\text{cap}} \tag{14}$$

The dynamics of the Li-Ion battery are described in Equation 15.

$$\frac{dE_{LI}(t)}{dt} = \eta_{LI}^{ch} P_{LI}^{ch}(t) - \frac{1}{\eta_{dis}^{LI}} P_{LI}^{dis}(t)(t) \tag{15}$$

$$0 \leq E_{LI}(t) \leq S_{LI} \tag{16}$$

$$0 \leq P_{LI}^{ch}(t),\ P_{LI}^{dis}(t)(t) \tag{17}$$

While the dynamics of the CB are described in Equation 18. Here, E_{TES} resembles the thermal energy stored in the TES.

$$\frac{dE_{TES}(t)}{dt} = -k_{loss} E_{TES}(t) + COP_{HP}(T_{cold}(t))\, P_{HP}(t) - \frac{1}{\eta_{ORC}(T_{cold})} P_{ORC}(t) \tag{18}$$

The operating range of the HP and ORC is expressed in equation 19.

$$\alpha_{HP}^{\text{lower}}\, S_{HP}^{\text{nom}} \leq P_{HP}(t) \leq \alpha_{HP}^{\text{upper}}\, S_{HP}^{\text{nom}} \tag{19}$$

$$\alpha_{ORC}^{\text{lower}}\, S_{ORC}^{\text{nom}} \leq P_{ORC}(t) \leq \alpha_{ORC}^{\text{upper}}\, S_{ORC}^{\text{nom}} \tag{20}$$

The variable α governs the bandwidth of operation that arises due to the compressor, expander and the chosen sizes of the heat exchangers. The start-up time to steady state for any technology is not considered as it is relatively small with respect to the large-scale duration of its operation. As the optimal dispatch problem is a Non-linear Optimization Problem (NLP), the interior point method from MadNLP.jl [24], [25] is used. The non-linearity majorly arises from the CB dynamics and the constrained physical sizes. The schematic of the solver is shown in figure 6.

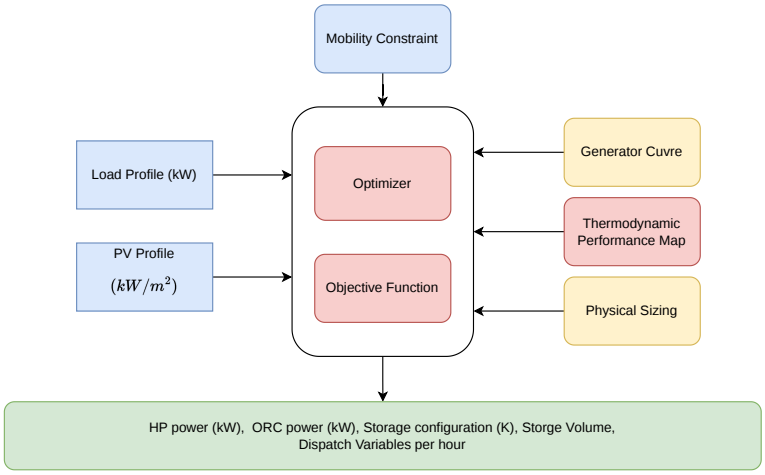

Figure 6: High Level Solver Framework

3. Test Case

The methodology described above is applied to analyze a fictional case with a 7-day time horizon. An installation of 650 m^2 of PV capacity is considered. A representative load demand profile is used, as shown in Figure 7. The HP source temperature is fixed at 300 K, and the ORC sink temperature at 280 K, as described in Section 2.2.. This difference of 20 K is considered as a approximation between the day and night temperatures differences.

For the optimal dispatch, the objective function is defined to minimize the camp's fuel consumption, as described in Equation 9. The fuel consumption is normalised with respect to the worst-case scenario, i.e., the case without any storage. The logarithm of this normalised value is then taken to improve numerical stability. The objective function of the optimal dispatch is described in Equation 9.

For the analysis, two cases are considered: lithium-ion storage capacities of 0 kWh and 30 kWh. The mass capacity of the energy storage container is varied from 500 kg to 1500 kg. The remaining parameters are provided in Table 1.

Table 1: Camp's and component Parameters

Δ Time Step	ρ_{Li}	$C_{p,water}$	Storage Wall thickness	k_{loss}	Max TES Volume
1.0 hr	7.6 $\frac{kg}{kWh}$	1.16 $\times 10^{-3}$ $\frac{kWh}{K \cdot Kg}$	4 $\times 10^{-3}$m	0.01 hr^{-1}	30m^3

The Figures 8–13 illustrate the evolution of the optimal sizing of the CB units. In general, the trend can be described as follows: as long as storage capacity (e.g., mass or TES volume) is not limiting,

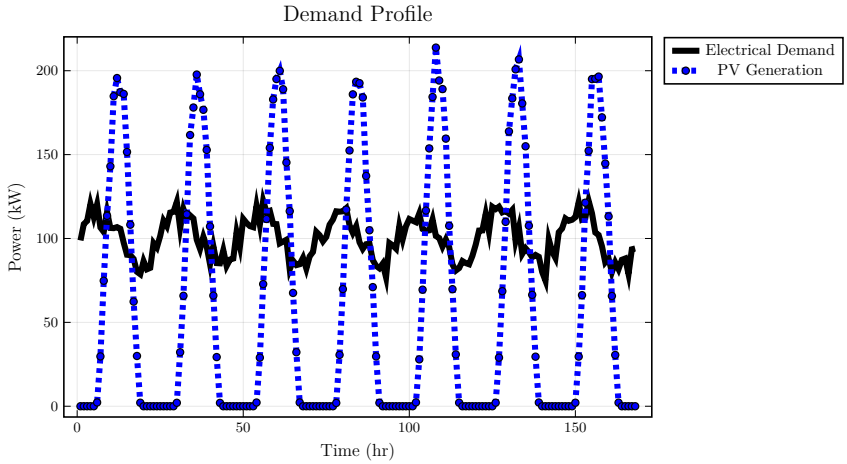

Figure 7: Electricity demand and PV generation over the simulation horizon

the optimization favors the most efficient CB configuration. However, once one or more constraints become active, the solution shifts to exploiting the Pareto front of the CB density–efficiency trade-off, as shown in Figure 5.

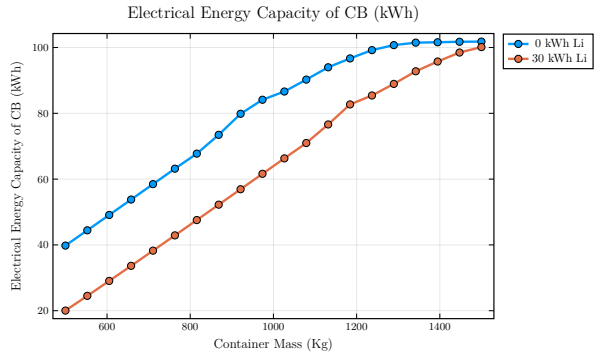

Figure 8: Optimal Electricity Energy Capacity of Carnot Battery for the container

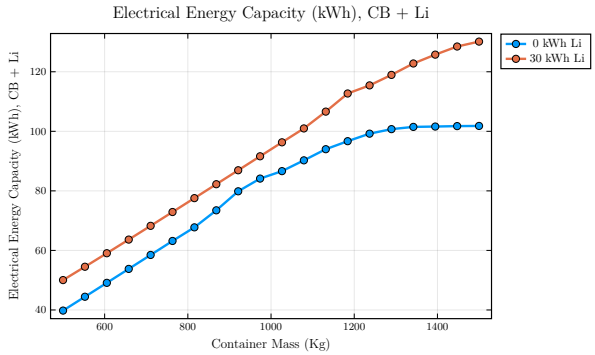

Figure 9: Optimal Electricity Energy Capacity of the energy storage container

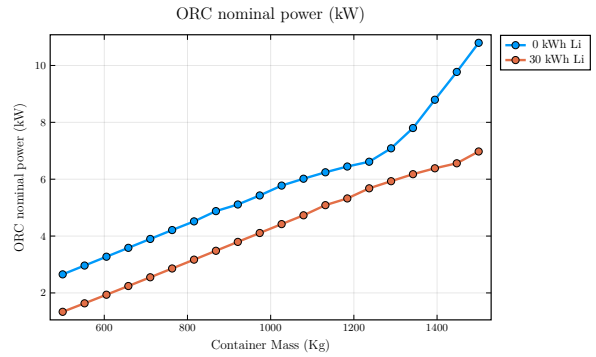

Figure 10: Nominal power of ORC

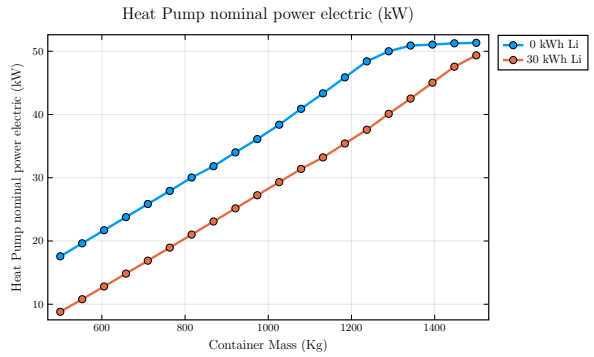

Figure 11: Nominal electrical power of HP

Between the two test cases, the optimization generally prefers the lithium-ion battery due to higher efficiency. As a result, the total energy storage capacity of the container is consistently higher when lithium-ion storage is included. Nevertheless, the difference between the two cases can be considered competitive (Figure 9). This behaviour arises from the optimal dispatch and sizing of the system components within the camp.

As the carrying capacity of the system increases, the sizes of all Carnot Battery components (HP–TES–ORC) generally increase. This scaling has only a minimal impact on the round-trip efficiency until one of the system constraints becomes active. In this case, the limiting factor is the maximum allowable

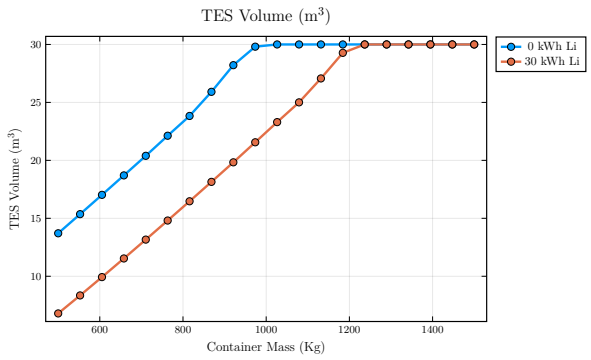

Figure 12: Volume of TES

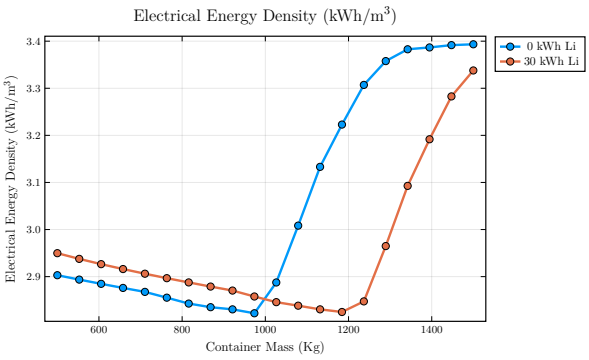

Figure 13: Energy Density of CB

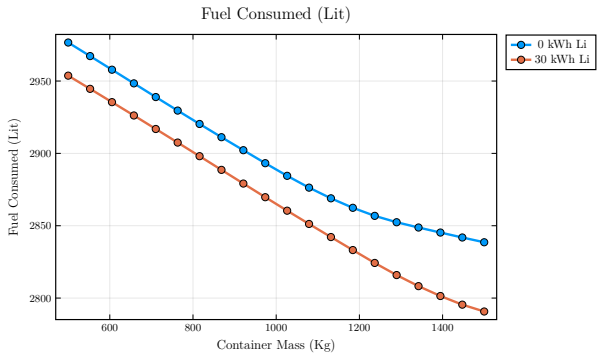

Figure 14: Fuel Consumption over time horizon

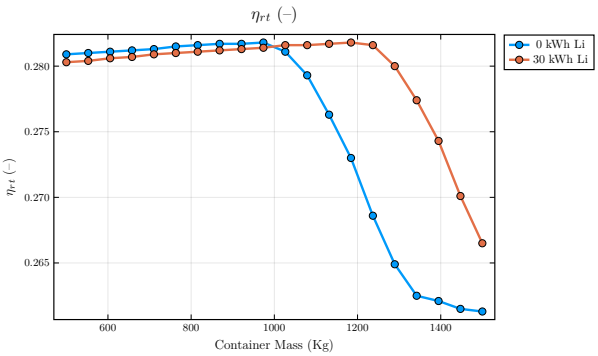

Figure 15: Round Trip Efficiency of CB

storage volume (30 m^3), as evidenced in Figures 13, 12, and 15.
The fuel consumption of the camp decreases progressively as the allowable carrying capacity increases, as shown in Figure 14. This highlights the benefit of increased storage capacity in reducing reliance on fuel-based generation.
Since the objective of the system is purely electrical supply, the ORC plays a critical role in the overall performance. In certain cases, the optimization favours increasing the ORC capacity without a corresponding increase in the HP capacity. This behaviour is observed in Figures 10 and 11, particularly when the carrying capacity exceeds 1400 kg.

For all the cases analysed, the ORC was able to meet only between 1% - 4% of the demand, Figure 16. This is still marginal to the system after considering the net fuel reduction to lie between 2% - 3%.

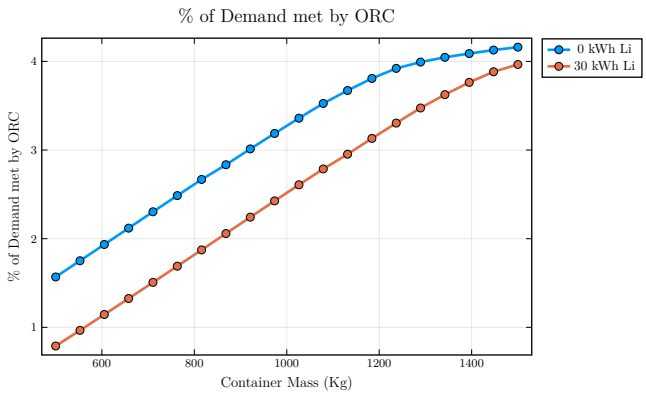

Figure 16: Fraction of energy met by the ORC

4. Conclusion

This work establishes a link between the thermodynamic design of Carnot Batteries (CB) and their role within large-scale, mobile microgrid energy systems. In particular, it demonstrates how microscopic thermodynamic variables mainly the storage temperature configurations influence system-level design decisions relevant to mobile camps.

The results highlight that the density–efficiency trade-off of the Carnot Battery plays a critical role in system sizing. Under mass and volume constraints, energy density emerges as a more influential parameter than round-trip efficiency. Consequently, the optimal thermodynamic design point remains relatively stable in terms of efficiency, while shifting significantly in terms of energy density as container constraints become more restrictive. Only when the maximum allowable thermal energy storage (TES) volume is reached does the thermodynamic efficiency begin to significantly impact system performance.

From a system perspective, the sizing of HP and ORC units is strongly governed by dispatch dynamics and the non-linear interactions within the system. The results show that both HP and ORC capacities tend to increase when excess energy is available for storage. However, due to the relatively low round-trip efficiency of CB, the optimization framework prioritizes lithium-ion storage, with CB integration becoming relevant primarily when lithium-ion capacity limits are reached.

Furthermore, the strong non-linearity of the system leads to non-intuitive design trade-offs. In certain scenarios, the optimization favors increasing ORC capacity while maintaining constant HP capacity to minimize fuel consumption. In other cases, slight reductions in storage capacity are accepted to achieve better sizing of HP and ORC units. Notably, ORC capacity is rarely sacrificed, indicating its critical role in energy recovery within the system.

Overall, this study demonstrates that Carnot Battery integration in mobile microgrids is highly context-dependent, with its relevance emerging under specific operational and constraint-driven conditions arising from mobility of the unit. About 2% of fuel reduction was achieved over the 7 day horizon. The current work also only focusses on electrification without any consideration of thermal loads of the camp. This significantly downplays the importance of the Carnot Battery. Hence the future work should contain:

- Integration of generator waste heat into the Carnot Battery system.
- Coupled optimization of electrical and thermal loads.
- Impact of ambient conditions on system performance
- Identification and evaluation of Carnot Battery sub-technologies best suited for mobile camp applications.

Nomenclature

PV	Photovoltic panels
HP	Heat Pump
COP	Coefficient of Performance
TES	Thermal Energy Storage
Li	Lithium Ion Battery
ORC	Organic Rankine Cycle
h	specific enthalpy, $\mathrm{J/kg}$
c_p	specific heat, $\mathrm{kWh/(kgK)}$
P	Power, kW
E	Energy, kWh
S	Energy Size of unit
z	mole fraction, (-)

T temperature, (K)
$\dot{Q}$ Heat transfer Rate, (kW)
$\dot{W}$ Power, (kW)

Greek symbols

η efficiency
α Operation range factor

Subscripts and superscripts

sh super-heat
sc sub-cool
comp compressor
exp expander
cond condenser
evap evaporator
rt round trip
cold cold store temperature
hot hot store temperature
ch charge
dis discharge
pp pinch point

References

[1] Dumont, O., Charalampidis, A., Lemort, V., Karellas, S., 2021. Experimental investigation of a thermally integrated carnot battery using a reversible heat pump/organic rankine cycle. URL: https://docs.lib.purdue.edu/iracc.

[2] Dumont, O., Lemort, V., 2020. Mapping of per- formance of pumped thermal energy storage (carnot battery) using waste heat recovery. Energy 211. doi:10.1016/j.energy.2020.118963.

[3] Eddy, J., Miner, N.E., Stamp, J., 2017. Sandia's microgrid design toolkit. The Electricity Journal 30, 62–67. URL: https://www.sciencedirect.com/science/article/pii/S1040619017300544, doi:https://doi.org/10.1016/j.tej.2017.04.002. special Issue: Contemporary Strategies for Microgrid Operation & Control.

[4] HOMER Energy, 2026. HOMER Pro. URL: https://www.homerenergy.com/. hybrid renewable and distributed generation system design software.

[5] de Godoy Antunes, E., Haessig, P., Wang, C., Leborgne, R.C., 2022. Optimal microgrid sizing using gradient-based algorithms with automatic differentiation, in: 2022 IEEE PES Innovative Smart Grid Technologies Conference Europe (ISGT-Europe), pp. 1–6. doi:10.1109/ISGT-Europe54678.2022.9960498.

[6] Laterre, A., 25 June 2025. Carnot batteries for heat and power coupling: Energy, Exergy, Economic and Environmental (4E) analysis. Ph.D. thesis. univeristy of Liege.

[7] Lubin, M., Dowson, O., Dias Garcia, J., Huchette, J., Legat, B., Vielma, J.P., 2023. JuMP 1.0: Recent improve ments to a modeling language for mathematical optimization. Mathematical Programming Computation 15, 581–589. doi:10.1007/s12532-023-00239-3.

[8] MicroGridsPy Contributors, 2026. MicroGridsPy: An open- source optimization model for microgrid sizing and dispatch. https://github.com/MicroGridsPy/MicroGridsPy. URL: https://github.com/MicroGridsPy/MicroGridsPy. accessed: 19 January 2026

[9] Deshpande, S., Janssens, B., 2025. ThermoCycleGlides.jl: Nonlinear pinch point solver for

hp-orc systems. https://github.com/Sush1090/ThermoCycleGlides.jl. Commit version used: v0.2.12 (latest as of Mar 20, 2026).

[10] Yew, P.J.W.H.W., Riedemann, A., 2022. Clapeyron.jl: An extensible, open-source fluid thermodynamics toolkit. Ind. Eng. Chem. Res. 61, 7130–7153. URL: https://pubs.acs.org/doi/10.1021/acs.iecr.2c00326, doi:doi/10.1021/acs.iecr.2c00326.

[11] European Defence Fund. *INDY - Energy Independent and Efficient Deployable Military Camps* Available at: https://defence-industry-space.ec.europa.eu/document/download/f2fefde8-bdef-4c76-914b-b7b040a2a988_en?filename=Factsheet_EDF21_INDY.pdf.

[12] European Defence Fund. *NOMAD - NOvel energy storage technologies usable at MilitAry Deployments in forward operating bases* Available at: https://defence-industry-space.ec.europa.eu/document/download/ae407ddb-2ad9-4b98-a66a-1732d11e9f95_en?filename=Factsheet_EDF21_NOMAD.pdf.

[13] European Defence Fund. *SENTINEL - Sustainable Energy Capabilities for Enhanced Military Camps and Operations* Available at: https://defence-industry-space.ec.europa.eu/document/download/3bb03680-d415-47a7-a470-3e0a781a298a_en?filename=FACTSHEET_EDF_2024_DA_ENERENV_EEMC_STEP_101224400_SENTINEL.pdf.

[14] Piña-Martinez, A., Privat, R., Nikolaidis, I.K., Economou, I.G., Jaubert, J.N., 2021. What is the optimal activity coefficient model to be combined with the translated–consistent peng–robinson equation of state through advanced mixing rules? cross-comparison and grading of the wilson, uniquac, and nrtl ae models against a benchmark database involving 200 binary systems. Industrial & Engineering Chemistry Research 60, 17228–17247. URL: https://doi.org/10.1021/acs.iecr.1c03003, doi:10.1021/acs.iecr.1c03003, arXiv:https://doi.org/10.1021/acs.iecr.1c03003.

[15] ENOGIA, n.d. Organic Rankine Cycle (ORC) solutions. URL: https://enogia.com/en/en-orc/ (accessed 2026-03-20).

[16] German Generator GmbH, n.d. Industrial power generators. URL: https://germangenerator.com/products/industrial-power-generators/ (accessed 2026-03-20).

[17] Copeland, n.d. Copeland select software. URL: https://www.copeland.com/en-gb/tools-resources/copeland-select-software (accessed 2026-03-20).

[18] Global Power Supply, n.d. Power kVA to kW calculator. URL: https://www.globalpwr.com/power-kva-kw-calculator/ (accessed 2026-03-20).

[19] Roy, S., Diaz, G., Winston, R., Palko, J.W., 2023. Packed bed thermal energy storage system using form-stable high-density polyethylene. Applied Thermal Engineering 218, 119209. URL: https://doi.org/10.1016/j.applthermaleng.2022.119209, doi:10.1016/j.applthermaleng.2022.119209.

[20] Bezanson, J., Edelman, A., Karpinski, S., Shah, V.B., 2017. Julia: a fresh approach to numerical computing. SIAM Review 59, 65–98. URL: https://epubs.siam.org/doi/10.1137/141000671, doi:10.1137/141000671.

[21] Mejía-de-Dios, J.A., Mezura-Montes, E., 2022. Metaheuristics: a Julia package for single- and multi-objective optimization. Journal of Open Source Software 7, 4723. URL: https://doi.org/10.21105/joss.04723, doi:10.21105/joss.04723.

[22] Zühlsdorf, B., Jensen, J.K., Cignitti, S., Madsen, C., Elmegaard, B., 2018. Analysis of temperature glide matching of heat pumps with zeotropic work-

ing fluid mixtures for different temperature glides. Energy 153, 650–660. URL: https://www.sciencedirect.com/science/article/pii/S0360544218306522, doi:10.1016/j.energy.2018.04.048.

[23] Andreasen, J.G., Larsen, U., Knudsen, T., Haglind, F., 2015. Design and optimization of a novel organic Rankine cycle with improved boiling process. Energy 91, 48–59. URL: https://www.sciencedirect.com/science/article/pii/S0360544215008786, doi:10.1016/j.energy.2015.06.122.

[24] Shin, S., Anitescu, M., Pacaud, F., 2024. Accelerating optimal power flow with GPUs: SIMD abstraction of nonlinear programs and condensed-space interior-point methods. Electric Power Systems Research 236, 110651.

[25] Shin, S., Coffrin, C., Sundar, K., Zavala, V.M., 2021. Graph-based modeling and decomposition of energy infrastructures. IFAC-PapersOnLine 54, 693–698.